Conformal Functionalization of Cotton Fibers via Isoreticular Expansion of UiO-66 Metal-Organic Frameworks

Marion Schelling [1], Eugenio Otal [2], Manuela Kim [2] and **Juan P. Hinestroza [1],***

[1] Department of Fiber Science, Cornell University, Ithaca, NY 14853, USA; ms2567@cornell.edu
[2] Department of Chemistry and Materials, Faculty of Textile Science and Technology, Shinshu University, Ueda Campus, Nagano 386-0018, Japan; eugenio_otal@shinshu-u.ac.jp (E.O.); manuela_kim@shinshu-u.ac.jp (M.K.)
* Correspondence: jh433@cornell.edu; Tel.: +1-607-255-7600

Abstract: We report on the growing of metal-organic frameworks that are isoreticular and isostructural to UiO-66, onto cotton fabrics via a solvothermal method. Four different metal-organic frameworks (MOFs) (UiO-66, UiO-66-NH$_2$, UiO-66-NDC, and UiO-67) were chosen as a case study. The presence of the UiO-based MOFs was confirmed through X-ray diffraction and Scanning Electron Microscopy. We used thermogravimetric analysis to quantify the amount of the MOF loading, which ranged from 0.8% to 2.6% m/m. We also explored the role of ligand size, growth time, and reaction temperature on the conformal coating of cotton fibers with these Zr-based MOFs. Cotton fabrics coated with Zr-based MOFs can find applications as selective filters in aggressive environments due to their enhanced chemical and thermal stabilities.

Keywords: cotton; metal-organic framework; UiO-66; UiO-67

1. Introduction

Since their discovery over 20 years ago, more than 75,000 different metal-organic framework (MOF) structures have been synthesized, which makes them one of the most reported materials in the 21st century's scientific literature [1]. MOFs are highly crystalline and porous materials composed of metal ions or cluster cornerstones linked by organic molecules [2]. Applications for MOFs, such as gas storage [3–7], catalysis [8–11], and photocatalysis [12–14], are limited by the thermal, mechanical, and chemical stability of the MOF structures. UiO-66, a MOF that contains a Zr$_6$O$_4$(OH)$_4$ cluster coordinated to carboxyl groups, is thermally stable up to 500 °C and chemically stable in water over a wide range of pH values [15–17].

The isoreticular concept originates from the Greek "*iso*" meaning "*same*" and from the Latin "*reticulum*" meaning "*net*" or "*network*" [18], and refers to the expansion of a unit cell. In the particular case of UiO-66, isoreticular growth refers to an increase in the distances between Zr$_6$O$_4$(OH)$_4$ clusters, while keeping the connectivity between the metal oxide cornerstones and the ligands. Isoreticular chemistry is of great relevance, as it can dictate the pore size of the resulting MOF structure [19–23].

The first reported synthesis of UiO-66 and its isoreticular counterpart UiO-67 by Lillerud et al. was reported in 2008 [15]. Five years later, the isostructural UiO-66-NH$_2$, in which terephthalic acid is replaced by 2-amino terephthalic acid, adding a -NH$_2$ moiety to the structure, was reported [24]. Reports on the synthesis of an intermediate member called UiO-66-NDC followed [25]. Ligand replacement can enhance hydrogen bonding [26] and catalytic activity [27] of the MOF. For example, substitution of terephthalic acid with 2,6-naphthalenedicarboxylic acid

(NDC) or 4,4'-dibenzoic acid (BPDC) results in an enhanced π–π stacking and a larger pore size [28]. Figure 1a shows a schematic of the structure of UiO-66 with the Zirconium oxide polyhedron forming the cornerstones and each metal oxide cornerstone coordinating with twelve terephthalic ligands. Terephthalic acid can be substituted with different ligands, as highlighted in Figure 1b–e, and it has been reported that the size and chemistry of the ligands have a significant impact on the kinetics of crystal growth [29].
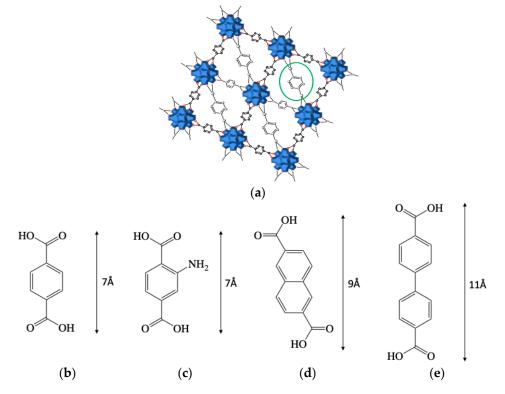

(a)

(b) **(c)** **(d)** **(e)**

Figure 1. Isoreticular UiO-metal-organic frameworks (MOFs): (**a**) schematic representation of UiO-66. Zirconium oxide cornerstones are shown in blue, and one of the ligands is highlighted in green; (**b**) terephthalic acid; (**c**) amino-terephthalic acid; (**d**) 2,6-naphthalenedicarboxylic acid; (**e**) 4,4'-dibenzoic acid.

Cotton fabrics are versatile in their fabric pore size, are biodegradable, and offer a flexible yet mechanically strong scaffolding structure to support MOFs in various environments. Potential applications for coated fabrics depend on the functionalization (i.e., type of MOF). In the literature, applications for MOF-functionalized fabrics range from filters [17,30] to sensors [31] and photocatalysts [32].

In a prior work, we reported on the functionalization of cotton with UiO-66 using carboxylated cotton substrates [17]. In this manuscript, we focus on the isoreticular and isostructural growth of UiO-66 while bypassing the carboxylation step. We also show the effect of different reaction conditions on the properties of cotton fabrics functionalized with UiO-based MOFs. We grew the UiO-based structures without the aid of a binder, which was previously required to anchor Zr ions to textile substrates [33]. The optimized reaction pathways and reaction conditions are summarized in Figure 2 along with SEM images illustrating that the resulting cotton fibers are conformably coated with a thin layer of a UiO-based MOFs.
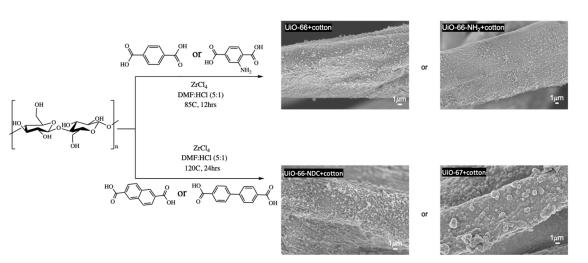
Figure 2. The two reaction paths used to deposit isoreticular UiO-based structures on cotton fibers.

2. Materials and Methods

2.1. Materials

Standardized cotton fabrics TIC-400 were obtained from Testfabrics, Inc. (West Pittston, PA, USA) and were cut into 2×2 cm^2 squares using a laser cutter. All chemicals were purchased from commercial sources and were used without further purification. Zirconium (IV), chloride (ZrCl$_4$, ≥99.5%; Aldrich, St. Louis, MO, USA), terephthalic acid (H$_2$BDC, 98%; Alfa Aesar, Haverhill, MA, USA), 2-Aminoterephthalic acid (BDC-NH$_2$, 99%, Alfa Aesar, Haverhill, MA, USA), naphthalene-2,6-dicarboxylic acid (98%, Aldrich, St. Louis, MO, USA), 4,4-dibenzoic acid (Biphenyl-4,4′-dicarboxylic acid, 97%, Aldrich, St. Louis, MO, USA), *N,N*-dimethylformamide (DMF; Mallinckrodt Chemicals, Phillipsburg, NJ, USA), hydrochloric acid (HCl, 36.5%–38%; Alfa Aesar, Tewksbury, MA, USA), deionized (DI) water, sodium hydroxide (NaOH pellets; Macron, Atlanta, GA, USA), non-ionic surfactant Triton X-100 (0.08%; Electron Microscopy Sciences, Hatfield, PA, USA), and acetic acid (Macron, Atlanta, GA, USA, glacial).

2.2. Methods

Cotton swatches were immersed in a scouring solution at 100 °C following a procedure reported in a previous manuscript [17]. Individual procedures for each one of the UiO-based structures are described below.

2.2.1. Cotton+UiO-66 and Cotton+UiO-66-NH$_2$

ZrCl$_4$ (0.55 mmol) was dissolved in a mixture of DMF:HCl (5mL:1mL). Using an ultrasonic bath, either H$_2$BDC (0.75 mmol) or BDC-NH$_2$ (0.75 mmol) were dissolved in 10 mL DMF. A scoured cotton swatch was added to the combined solution. The sealed containers were kept at 85 °C overnight and the functionalized fabrics were washed vigorously three times in DMF and deionized H$_2$O before being dried and conditioned at room temperature.

2.2.2. Cotton+UiO-66-NDC and Cotton+UiO-67

ZrCl$_4$ (0.55 mmol) was dissolved in a mixture of DMF:HCl (5 mL:1 mL). Either Naphthalene-2,6-dicarboxylic acid or 4,4-dibenzoic acid (0.75 mmol) were dissolved in 10 mL of DMF. A scoured cotton swatch was added to the combined solutions. The sealed containers were kept at 120 °C for 24 h, and the functionalized fabrics were washed vigorously three times in DMF and deionized H$_2$O before being dried and conditioned at room temperature for characterization.

2.2.3. Characterization of the Samples

X-ray diffraction (XRD) experiments were performed on a Bruker (Madison, WI, USA) D8 powder diffractometer with a step size of 0.04°. Scanning electron microscopy (SEM) was performed on a LEO 1550 FESEM (Keck SEM, Maple Grove, MN, USA). Prior to imaging, the specimens were coated with a thin layer of carbon. Thermograms were obtained using a TGA 550 thermal analyzer (TA Instruments, New Castle, DE, USA, heating rate of 10 °C/min) in air.

3. Results

We bypassed the cellulose carboxylation step commonly reported as a necessary condition for growth MOF structures onto cotton fibers, showing that MOFs can be grown directly onto unmodified cotton fibers. We observed that longer ligands (naphthalene-2,6-dicarboxylic acid and 4,4-dibenzoic acid) required of higher temperatures and longer reaction times to grow on the surface of the cotton fabrics. At 85 °C and 12 h, UiO-66-NDC and UiO-67 did not precipitate and the cotton fibers showed no evidence of crystal growth on their surfaces. However, when the reaction conditions were modified according to Butova et al. [34], that is to say, the temperature was increased from 85 °C to 120 °C and the growth time is increased from 12 h to 24 h, UiO-based structures were observed on the surface of the fabrics. Ragon et al. showed that not only does the availability of the inorganic cluster highly influence the crystallization rate [35], but also the kinetics of MOF growth become slower when the size of the ligand is longer [29].

The growth of isoreticular UiO-based MOFs on the surface of cotton fibers was confirmed using X-ray diffraction as shown in Figure 3. The bottom trace in Figure 3, corresponding to the scoured cotton specimen, exhibits broad diffraction peaks at 15°, 17°, and 23°, which are commonly assigned to cellulose I [36,37]. A clear superposition of the cellulose I diffraction peaks can be observed in the XRD spectra for all five specimens, indicating that the crystallinity of the cotton fibers was not modified during growth of the UiO-based MOFs. Furthermore, well defined diffraction peaks ascribed to Zirconium MOFs are observed at lower angles (between 5° and 14°). The pattern of the specimens quantitatively agrees with those reported in the literature for powdered UiO-66 [15], UiO-66-NDC [38], and UiO-67 [24], and also agrees with PXRD simulations of the respective MOFs showed in dotted lines in Figure 3. UiO-66-NH$_2$ is isostructural with UiO-66 [24]; therefore, the diffraction peaks for cotton+UiO-66 and cotton+UiO-66-NH$_2$ show the same diffraction peak positions. UiO-66-NDC and UiO-67 exhibit larger cell parameters, which is confirmed by the shifting of the diffraction peaks to lower angles.

The SEM images shown in Figure 4 illustrate the conformal surface coverage of the cotton fibers for all specimens. Figure 4A shows how crystals of UiO-67 form clusters of various sizes. Images of the cotton+UiO-67 and the cotton+UiO-66-NDC specimens show a uniform MOF layer that covers the cotton, and on top of that layer, additional crystalline structures are seen (Figure 4A–D). These node-like structures are also seen on the images of the cotton+UiO-66-NH$_2$ and the cotton+UiO-66 specimens (Figure 4E–H).

SEM images taken at higher magnifications confirm the coverage of the cotton's surface (Figure 4B,D,F,H). Cotton+UiO-66-NDC, cotton+UiO-66-NH$_2$, and cotton+UiO-66 specimens show a lower dispersion in particle size than the cotton+UiO-67 specimen. This observation can be explained on slower nucleation and growth kinetics. While MOFs with smaller ligands grow fast, the generation of nucleolus is instantaneous, and all these nucleoli grow simultaneously. Larger ligands hence generate a more polydisperse crystalline system [39].

Figure 5 shows the thermograms of the cotton fabrics coated with UiO-based MOF that were performed to quantify the amount of MOF growth onto each fabric. In the thermogram, a small weight loss between 30 and 100 °C, due to loss of water (3%–4%), is noted for all specimens. UiO-66-NH$_2$ exhibits a difference in the thermogram shape between 200 and 300 °C. This behavior was previously reported and could be related to the degradation of the amino group that is present only in this MOF [40]. Oxidative degradation of cellulose chains, resulting in combustion gases, is generally

observed between 300 and 650 °C, and char pyrolysis occurs at temperatures higher than 400 °C [41,42]. At temperatures ranging between 300 and 350 °C, dehydration of $Zr_6O_4(OH)_4$ to Zr_6O_6 occurs [24]. The thermogram of the cotton specimen shows a complete transformation into H_2O and CO_2 leaving less than 0.2% solid residue, which is used as reference for further calculations. Weight measurements between 700 and 900 °C indicate total degradation of cellulose and of the UiO66-based MOFs. Values of the residual mass of ZrO_2 left after the TGA experiments are shown in Table 1.

Table 1 presents the MOF formula for each specimen, the residue (% m/m), and the MOF loading. The residue column in Table 1 is the sum of the ash from the unmodified cotton specimen and the mass of ZrO_2. The ZrO_2 % in the specimen is calculated by subtracting the mass of the ash residue obtained from the ash generated by the untreated cotton. The mass of ZrO_2 residue is used to calculate the loading of the MOF using the MOF formula and assuming a complete transformation of that structure into CO_2, H_2O, and ZrO_2. The cotton+UiO-66-NH_2 specimen has the highest MOF loading, while the cotton specimen coated with UiO-67 exhibited the lowest weight residue, albeit being the heaviest of all MOFs used in this study.
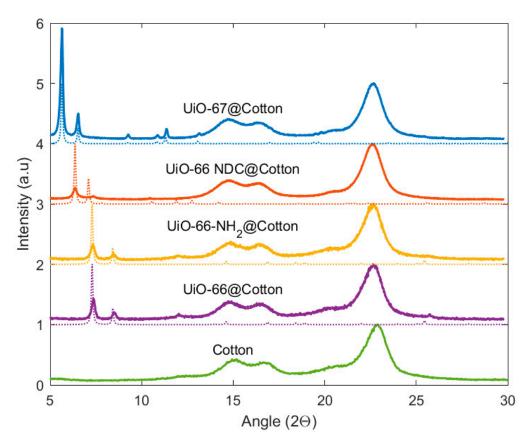

Figure 3. Solid lines: measured X-ray diffraction patterns for cotton+UiO-67 (blue), cotton+UiO-66-NDC (red), cotton+UiO-66-NH_2 (yellow), cotton+UiO-66 (violet), and cotton (green) specimens. In dotted lines are the respective simulated diffraction patterns of a corresponding MOF structure.
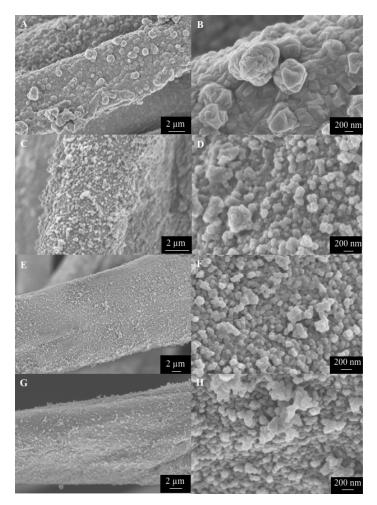
Figure 4. Scanning electron microscopy images of (**A**) cotton+UiO-67; (**B**) magnified image of cotton+UiO-67, showing the MOF immobilized onto the fiber; (**C**) cotton+UiO-66-NDC; (**D**) magnified segment of cotton+UiO-66-NDC; (**E**) cotton+UiO-66-NH$_2$; (**F**) magnified image of cotton+UiO-66-NH$_2$; (**G**) cotton+UiO-66 fiber; and (**H**) magnified segment of cotton+UiO-66 fiber.

Table 1. MOF formula, residue %, and MOF loading calculations for all specimens.

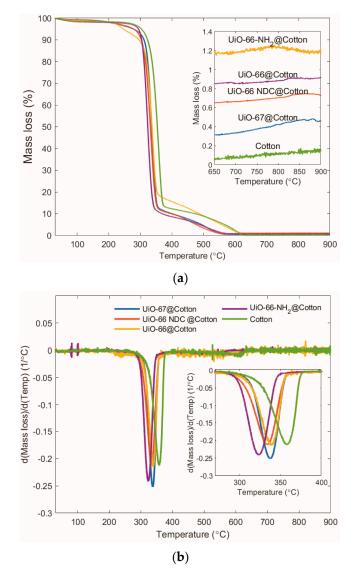| Sample Name	Mof Formula	Residue % M/M	MOF % M/M
cotton	–	0.20	–
Cotton+UIO-66	$Zr_{24}C_{192}H_{112}O_{128}$	0.91	1.6
Cotton+UIO-66-NH$_2$	$Zr_{24}C_{192}H_{136}O_{128}N_{24}$	1.19	2.3
Cotton+UIO-66-NDC	$Zr_{24}C_{288}H_{160}O_{128}$	0.73	1.4
Cotton+UIO-67	$Zr_{24}C_{336}H_{208}O_{128}$	0.45	0.72

(**a**)

(**b**)

Figure 5. (**a**) Thermogravimetric analysis of the cotton fabrics coated with UiO-Based MOFs showing the full temperature range from 30 to 900 °C. Insert: magnification for the 650 to 900 °C temperature range. (**b**) Differential Thermogravimetric analysis spectra. Insert: magnification for the 250 to 400 °C temperature range.

4. Conclusions

Cotton fibers were successfully coated with an isoreticular Zr-MOF series, namely, UiO-66, UiO-66-NH$_2$, UiO-66-NDC, and UiO-67, using a solvothermal method and without the need of prior functionalization of the cotton. Ligand solubility in DMF as well as particle formation kinetics appear to have the most impact in the growth of the UiO-based MOFs on the surface of cotton fibers. The growth of UiO-based MOFs was confirmed using XRD and SEM. The harsh washing of the specimens provides evidence that the coatings of UiO-based MOFs on the cotton fabrics are mechanically robust. The experimental results also offer evidence that solvothermal synthesis is an effective pathway for fabric functionalization and that with minor modifications in reaction time and reaction temperature, this method can be extended to an entire MOF family. Thermogravimetric analysis was used to determine the amount of loading on each fabric, which ranged from 0.8% to 2.6% We found that the larger the MOF structure, the lower the loading of the MOF on the fabric, which is in agreement with the need for longer growth times at higher temperatures to accelerate the kinetics and facilitate solubilization of the reagents. Further efforts are needed in order to understand

whether the thickness of the MOF coating is dependent on the availability of starting materials, on the thermodynamics of crystal growth or on steric restrictions. The reported method opens the possibility for a vast range of applications for functional fibers operating in aqueous environments under varying pH values and relatively high temperatures.

References

1. Caro, J. Quo vadis, MOF? *Chem. Ing. Tech.* **2018**, *90*, 1759–1768. [CrossRef]
2. Kaskel, S. *The Chemistry of Metal–Organic Frameworks: Synthesis, Characterization, and Applications*, 1st ed.; Wiley-VCH: Weinheim, Germany, 2016; Volume 1, pp. 1–3. [CrossRef]
3. Alezi, D.; Belmabkhout, Y.; Eddaoudi, M. MOF Crystal Chemistry Paving the Way to Gas Storage Needs: Aluminum-Based soc-MOF for CH_4, O_2, and CO_2 Storage. *J. Am. Chem. Soc.* **2015**, *137*, 11308–13318. [CrossRef] [PubMed]
4. Bonneau, M.; Lavenn, C.; Kitagawa, S. Upscale synthesis of a binary pillared layered MOF for hydrocarbon gas storage and separation. *Green Chem.* **2020**, *22*, 718–724. [CrossRef]
5. Connolly, B.; Madden, D.; Fairen-Jimenez, D. Shaping the Future of Fuel: Monolithic Metal–Organic Frameworks for High-Density Gas Storage. *J. Am. Chem. Soc.* **2020**, *142*, 8541–8549. [CrossRef] [PubMed]
6. Li, H.; Li, L.; Chen, B. Porous metal-organic frameworks for gas storage and separation: Status and challenges. *Energy Chem.* **2019**, *1*, 100006. [CrossRef]
7. Xue, D.-X.; Wang, Q.; Bai, J. Amide-functionalized metal–organic frameworks: Syntheses, structures and improved gas storage and separation properties. *Coord. Chem. Rev.* **2019**, *378*, 2–16. [CrossRef]
8. Kang, Y.-S.; Lu, Y.; Sun, W.-Y. Metal–organic frameworks with catalytic centers: From synthesis to catalytic application. *Coord. Chem. Rev.* **2019**, *378*, 262–280. [CrossRef]
9. Sharma, V.K.; Feng, M. Water depollution using metal-organic frameworks-catalyzed advanced oxidation processes: A review. *J. Hazard. Mater.* **2019**, *372*, 3–16. [CrossRef]
10. Konnerth, H.; Matsagar, B.; Wu, K.C.-W. Metal-organic framework (MOF)-derived catalysts for fine chemical production. *Coord. Chem. Rev.* **2020**, *416*, 213319. [CrossRef]
11. Xu, C.; Fang, R.; Li, Y. Functional metal–organic frameworks for catalytic applications. *Coord. Chem. Rev.* **2019**, *388*, 268–292. [CrossRef]
12. Li, F.; Wang, D.; Zou, J.-P. Design and syntheses of MOF/COF hybrid materials via postsynthetic covalent modification: An efficient strategy to boost the visible-light-driven photocatalytic performance. *Appl. Catal. B Environ.* **2019**, *243*, 621–628. [CrossRef]
13. Dong, D.; Yan, C.; Zhang, Z. An electron-donating strategy to guide the construction of MOF photocatalysts toward co-catalyst-free highly efficient photocatalytic H_2 evolution. *J. Mater. Chem. A* **2019**, *7*, 24180–24185. [CrossRef]
14. Mahmoodi, N.M.; Abdi, J. Nanoporous metal-organic framework (MOF-199): Synthesis, characterization and photocatalytic degradation of Basic Blue 41. *Microchem. J.* **2019**, *144*, 436–442. [CrossRef]
15. Cavka, J.H.; Jakobsen, S.; Olsbye, U.; Guillou, N.; Lamberti, C.; Bordiga, S.; Lillerud, K.P. A New Zirconium Inorganic Building Brick Forming Metal Organic Frameworks with Exceptional Stability. *J. Am. Chem. Soc.* **2008**, *130*, 13850–13851. [CrossRef] [PubMed]
16. Jiang, H.-L.; Feng, D.; Wang, K.; Gu, Z.-Y.; Wei, Z.; Chen, Y.-P.; Zhou, H.-C. An Exceptionally Stable, Porphyrinic Zr Metal–Organic Framework Exhibiting pH-Dependent Fluorescence. *J. Am. Chem. Soc.* **2013**, *135*, 13934–13938. [CrossRef] [PubMed]

17. Schelling, M.; Kim, M.; Otal, E.; Hinestroza, J.-P. Decoration of Cotton Fibers with a Water-Stable Metal–Organic Framework (UiO-66) for the Decomposition and Enhanced Adsorption of Micropollutants in Water. *Bioengineering* **2018**, *5*, 14. [CrossRef]

18. Ockwig, N.W.; Allendorf, M.D. Cobalt based isoreticular metal-organic frameworks (IRMOFs): A theoretical study on viability and stability. In Proceedings of the 211th ECS Meeting, Chicago, IL, USA, 6–10 May 2007.

19. Furukawa, H.; Go, Y.B.; Ko, N.; Park, Y.K.; Uribe-Romo, F.J.; Kim, J.; O'Keeffe, M.; Yaghi, O.M. Isoreticular Expansion of Metal–Organic Frameworks with Triangular and Square Building Units and the Lowest Calculated Density for Porous Crystals. *Inorg. Chem.* **2011**, *50*, 9147–9152. [CrossRef]

20. Zhou, H.-C.; Kitagawa, S. Metal–Organic Frameworks (MOFs). *Chem. Soc. Rev.* **2014**, *43*, 5415–5418. [CrossRef]

21. Eddaoudi, M.; Kim, J.; Rosi, N.; Vodak, D. Systematic design of pore size and functionality in isoreticular MOFs and their application in methane storage. *Science* **2002**, *295*, 469–472. [CrossRef]

22. Razavi, S.A.A.; Masoomi, M.Y.; Islamoglu, T.; Morsali, A.; Xu, Y.; Hupp, J.T.; Farha, O.K.; Wang, J.; Junk, P.C. Improvement of Methane–Framework Interaction by Controlling Pore Size and Functionality of Pillared MOFs. *Inorg. Chem.* **2017**, *56*, 2581–2588. [CrossRef]

23. Chen, X.; Peng, Y.; Cui, Y. Sixteen isostructural phosphonate metal-organic frameworks with controlled Lewis acidity and chemical stability for asymmetric catalysis. *Nat. Commun.* **2017**, *8*, 2171. [CrossRef] [PubMed]

24. Katz, M.J.; Brown, Z.J.; Colon, Y.J.; Siu, P.W.; Scheidt, K.A.; Snurr, R.Q.; Hupp, J.T.; Farha, O.K. A facile synthesis of UiO-66, UiO-67 and their derivatives. *Chem. Commun.* **2013**, *49*, 9449. [CrossRef] [PubMed]

25. Garibay, S.J.; Cohen, S.M. Isoreticular synthesis and modification of frameworks with the UiO-66 topology. *Chem. Commun.* **2010**, *46*, 7700–7702. [CrossRef] [PubMed]

26. Cmarik, G.E.; Kim, M.; Cohen, S.M.; Walton, K.S. Tuning the Adsorption Properties of UiO-66 via Ligand Functionalization. *Langmuir* **2012**, *28*, 15606–15613. [CrossRef] [PubMed]

27. Gomes-Silva, C.; Luz, I.; Llabres i Xamena, F.X.; Corma, A.; Garcia, H. Water Stable Zr–Benzenedicarboxylate Metal–Organic Frameworks as Photocatalysts for Hydrogen Generation. *Chem. Eur. J.* **2010**, *16*, 11133–11138. [CrossRef]

28. Yuan, S.; Feng, L.; Zhou, H.-C. Stable Metal-Organic Frameworks: Design, Synthesis, and Applications. *Adv. Mater.* **2018**, 30. [CrossRef]

29. Ragon, F.; Chevreau, H.; Devic, T.; Serre, C.; Horcajada, P. Impact of the Nature of the Organic Spacer on the Crystallization Kinetics of UiO-66(Zr)-Type MOFs. *Chem. Eur. J.* **2015**, *21*, 7135–7143. [CrossRef]

30. Lopez-Maya, E.; Montoro, C.; Rodriguez-Albelo, L.M.; Aznar Cervantes, S.D.; Lozano-Perez, A.A.; Cenis, J.L.; Barea, E.; Navarro, J.A.R. Textile/Metal–Organic-Framework Composites as Self-Detoxifying Filters for Chemical-Warfare Agents. *Angew. Chem. Int. Ed.* **2015**, *54*, 1–6. [CrossRef]

31. Rauf, S.; Vijjapu, M.T.; Andres, M.A.; Gascon, I.; Roubeau, O.; Eddaoudi, M.; Salama, K.N. A Highly Selective Metal-Organic Framework Textile Humidity Sensor. *Acs Appl. Mater. Interfaces* **2020**, *26*, 29999–30006. [CrossRef]

32. Lee, D.T.; Jamir, J.D.; Peterson, G.W.; Parsons, G.N. Protective Fabrics: Metal-Organic Framework Textiles for Rapid Photocatalytic Sulfur Mustard Simulant Detoxification. *Matter* **2020**, *2*, 404–415. [CrossRef]

33. Bunge, M.A.; Davis, A.B.; West, K.N.; West, C.W.; Glover, T.G. Synthesis and Characterization of UiO-66-NH2 Metal–Organic Framework Cotton Composite Textiles. *Ind. Eng. Chem. Res.* **2018**, *57*, 9151–9161. [CrossRef]

34. Butova, V.V.; Budnyk, A.P.; Lamberti, C. Modulator effect in UiO-66-NDC (1,4-naphthalenedicarboxilic acid) synthesis and comparison with UiO-67-NDC isoreticular MOFs. *Cryst. Growth Des.* **2017**, *17*, 5422–5431. [CrossRef]

35. El Osta, R.; Feyand, M.; Walton, R.I. Crystallisation Kinetics of Metal Organic Frameworks from in situ Time-Resolved X-ray Diffraction. *Powder Diffr.* **2013**, *28*, S256. [CrossRef]

36. French, A.D. Idealized powder diffraction patterns for cellulose polymorphs. *Cellulose* **2014**, *21*, 885–896. [CrossRef]

37. Segal, L.; Creely, J.J.; Martin, A.E.; Conrad, C.M. An Empirical Method for Estimating the Degree of Crystallinity of Native Cellulose Using the X-Ray Diffractometer. *Text. Res. J.* **1959**, *29*, 786–794. [CrossRef]

38. David, J.; Trolliard, G.; Volkringer, C.; Loiseau, T.; Maitre, A. Synthesis of zirconium oxycarbide powders using metal–organic framework (MOF) compounds as precursors. *RSC Adv.* **2015**, 51650–51661. [CrossRef]

39. Van Vleet, M.J.; Weng, T.; Schmidt, J.R. In Situ, Time-Resolved, and Mechanistic Studies of Metal–Organic Framework Nucleation and Growth. *Chem. Rev.* **2018**, 3681. [CrossRef]

40. Otal, E.H.; Kim, M.L.; Calvo, M.E.; Karvonen, L.; Fabregas, I.O.; Sierra, C.A.; Hinestroza, J.P. A panchromatic modification of the light absorption spectra of metal–organic frameworks. *Chem. Commun.* **2016**, *52*, 6665–6668. [CrossRef]

41. Loof, D.; Hiller, M.; Oschkinat, H.; Koschek, K. Quantitative and Qualitative Analysis of Surface Modified Cellulose Utilizing TGA-MS. *Materials* **2016**, *9*, 415. [CrossRef]

42. Zhu, P.; Sui, S.; Wang, B.; Sun, K.; Sun, G. A study of pyrolysis and pyrolysis products of flame-retardant cotton fabrics by DSC, TGA, and PY–GC–MS. *J. Anal. Appl. Pyrolysis* **2004**, *71*, 645–655. [CrossRef]